Green Chemistry

Cutting-edge research for a greener sustainable future

Accepted Manuscript

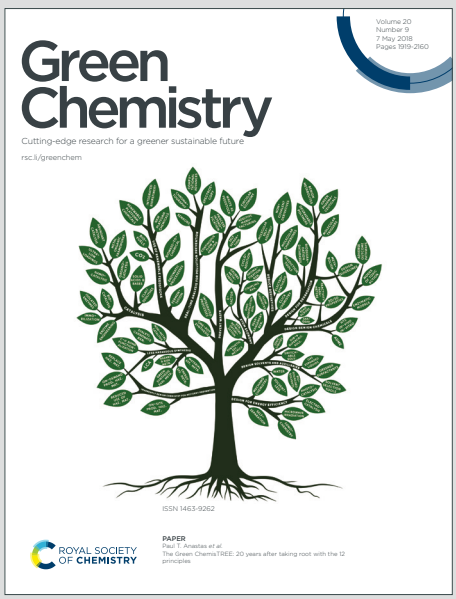

ROYAL SOCIETY OF CHEMISTRY

rsc.li/greenchem

View Article Online
DOI: 10.1039/D0GC00730G

View Article Online
DOI: 10.1039/D0GC00730G

COMMUNICATION

B-doped CuO nanobundles for electroreduction of carbon dioxide to ethylene

Received 00th January 20xx,
Accepted 00th January 20xx

DOI: 10.1039/x0xx00000x

Qiang Wan,[a] Jianling Zhang,*[a, b] Bingxing Zhang,[a] Dongxing Tan,[a] Lei Yao,[c] Lirong Zheng,[c] Fanyu Zhang,[a] Lifei Liu,[a] Xiuyan Cheng[a] and Buxing Han[a, b]

A novel boron-doped CuO nanobundles is designed for CO_2 reduction to the only multi-carbon product of ethylene and its faradaic efficiency can reach 58.4% with a current density of 18.2 mA cm^{-2}. The active, selective and simply prepared electrocatalyst provides a promising electrocatalyst candidate for CO_2 reduction to ethylene.

In recent years, the emission of carbon dioxide (CO_2) has brought huge impacts on global environment, such as melting of icebergs, rise of sea level, forest fires, extremely hot and cold weather and so on.[1-5] Therefore, how to utilize CO_2 and turn it into renewable carbon resources have become into a new trend.[6] Particularly, the electroreduction of CO_2 expands the range of chemical applications of CO_2 because it can run the reaction with Gibbs free energy both less than and higher than zero.[7] So far, the faradaic efficiency (FE) of low energy C1 products, represented by carbon monoxide and formic acid, is close to 100%,[8] while the FE values of multi-carbon products with higher values and energy are not high enough. Up to now, copper is one of the most efficient metals that can catalyze CO_2 into multi-carbon compounds owing to its appropriate adsorption and desorption energy for intermediates in CO_2 reduction reaction (CO_2RR) process.[8-13] Great efforts have been devoted to the efficient acquisition of multi-carbon products on copper catalysts, such as using noble metals to form alloys with copper,[14-18] adjusting crystal surface of copper catalyst[8,19-21] and heteroatom doping.[22-25] Among these studies, the incorporation of light element boron (B) into Cu catalyst has been reported to boost CO_2 conversion.[24,26] Even though the total FE of C2 hydrocarbons could reach ~80%[24] or 48.2%[26] at applied potentials, other C2 products (ethylene, ethanol, ethane) are generated simultaneously and the FE of ethylene were 52%[24] and 15.2%.[26] Recently, we reported the construction of multi-shelled CuO microboxes, which can convert CO_2 into ethylene with a maximum FE of 51.3% in 0.1 M K_2SO_4 solution[27]. It still remains a great challenge to selectively obtain a single multi-carbon product from electrocatalytic CO_2RR.

Herein, we propose for the first time the B-doped CuO nanobundles for highly efficient production of ethylene from electrocatalytic CO_2RR. Ethylene is the only multi-carbon product and its FE can reach 58.4% at -1.1 V (versus the reversible hydrogen electrode, *vs*. RHE) with a current density of 18.2 mA cm^{-2}. The B-doped CuO nanobundles have a nanowire stack structure and abundant oxygen vacancies, which increase the exposure of accessible active sites, CO_2 adsorption capacity and facilitate the diffusion of CO_2 and electrocatalytic product.

The catalyst was prepared by a simple method (Scheme S1). Typically, the desired amounts of copper chloride dihydrate, polyethylene glycol (PEG, average MW: 20000) and boric acid were dissolved in water, followed by addition of a certain amount of sodium hydroxide. PEG plays as a directing reagent for nanowire formation. After reaction for 2 h, the product was obtained by centrifugation, washing and drying. It is worth noting that such a wet chemical route for catalyst synthesis is simple, convenient, rapid and involves no calcination procedure that is usually requisite for the preparation of copper electrocatalysts[24,27].

Fig. 1 shows the characterizations of the catalyst with B content of 0.49 wt%, which was determined by inductively coupled plasma-atomic emission spectrometry (ICP-AES). It presents a spindle structure assembled by nanowires in length of 1 μm and width of 10 nm, as revealed by scanning electron microscopy (SEM) and transmission electron microscopy (TEM) (Fig. 1a-d). High-resolution TEM (HRTEM) image reveals an interplanar distance of 0.198 nm (Fig. 1e), corresponding to (11-1) plane of face centered Tenorite. Energy-dispersive X-ray spectroscopy (EDS) images (Fig. 1f) show the uniform distributions of copper and oxygen elements on nanowire, as well as a small amount of B. X-ray diffraction (XRD) pattern (Fig. 1g) presents two sharp diffractions at 35.4°, 38.7° and other diffractions at 48.7°, 58.2°, 61.5°, 65.8° and 66.2°, corresponding to (002), (11-1), (20-2), (202), (11-3), (022) and (31-1) planes of Tenorite, respectively (PDF #48-1548). For comparison, the B-free CuO was prepared by the method for B-doped CuO without boric acid addition, which shows a similar morphology with B-doped CuO (Fig. S1†). The B-doped CuO

[a] Beijing National Laboratory for Molecular Sciences, CAS Key Laboratory of Colloid, Interface and Chemical Thermodynamics, CAS Research/Education Center for Excellence in Molecular Sciences, Institute of Chemistry, Chinese Academy of Sciences, Beijing 100190, P.R.China.
[b] Physical Science Laboratory, Huairou National Comprehensive Science Center, Beijing 101400, P.R.China.
[c] Beijing Synchrotron Radiation Facility (BSRF), Institute of High Energy Physics, Chinese Academy of Sciences, Beijing 100049, P.R.China.

†Electronic Supplementary Information (ESI) available: See DOI: 10.1039/x0xx00000x

nanobundles and B-free CuO nanobundles are defined as B-CuO and CuO, respectively. Additionally, the commercial CuO was used for comparison, which presents microparticles in 0.5-4 μm (Fig. S2†).

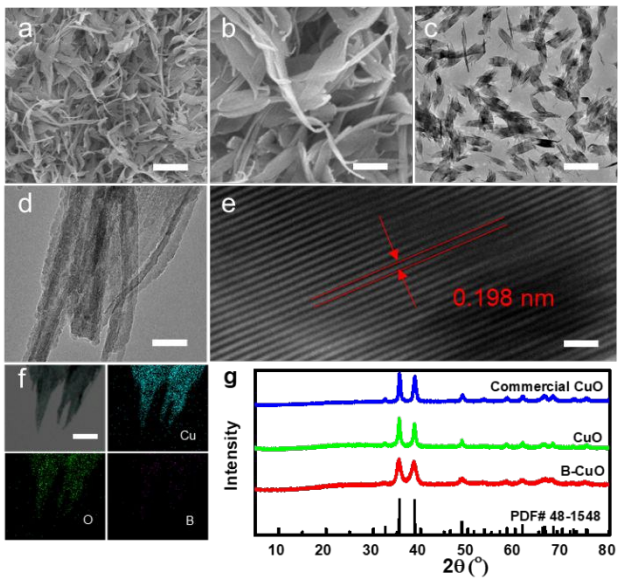

Fig. 1 SEM images (a, b), TEM images (c, d), HRTEM image (e) and EDS image (f) of B-CuO and XRD patterns of different catalysts (g). Scale bars: 800 nm in a, 200 nm in b, 400 nm in c, 50 nm in d, 1 nm in e, 120 nm in f.

Fourier transform infrared spectroscopy (FT-IR) was employed to probe the interaction between B and CuO in B-CuO (Fig. 2a and Fig. S3†). There are two absorptions at 1372 cm^{-1} and 1500 cm^{-1} for B-CuO (Fig. 2a), which are absent in CuO. It can be attributed to the symmetrical stretching vibration and asymmetric stretching vibration of B-O bond.[28-31] For O1s X-ray photoelectron spectroscopy (XPS), there are four peaks at 529.8 eV (red line), 530.5 eV (blue line), 531.5 eV (plum line) and 533.4 eV (green line) corresponding to Cu-O-Cu, B-O,[32-34] O-O and Cu-OH in B-CuO, respectively (Fig. 2b).[35-37] All these results prove the formation of B-O bond in B-CuO. For Cu2p XPS spectrum, there are two peaks corresponding to Cu^{2+} at 934.2 eV and 954.1 eV (Fig. S4†). To further detect the local structure of B-CuO at atomic level, the synchrotron X-ray absorption fine structure (XAFS) was determined. For comparison, the XAFS spectra of four contrast samples of CuO, commercial CuO, commercial cuprous oxide (Cu_2O) and Cu foil were determined. For Cu K-edge X-ray absorption near-edge structure (XANES, Fig. 2c), the absorption edge positions of B-CuO and CuO are located behind commercial Cu_2O and Cu foil and near that of commercial CuO, implying the valence of +2.[24] The radial distribution function (RDF) obtained from the fourier transform (FT) k^3-weighted normalized extended X-ray absorption fine structure (EXAFS) data (Fig. 2d) of commercial CuO shows a peak at 1.96 Å, corresponding to Cu-O coordination.[38-39] As for B-CuO, the intensity of peak for Cu-O bond increases, indicating the increased oxygen defect. Meanwhile, the peak at ~2.89 Å corresponding to Cu-Cu bond for B-CuO greatly reduced compared with commercial CuO. The coordination number of copper in B-CuO was determined to be 6.8, which is lower than those of CuO and commercial CuO (7.2 and 8 respectively, Table S1 †).[40] The results show that the introduction of B in CuO reduces the coordination number of copper.

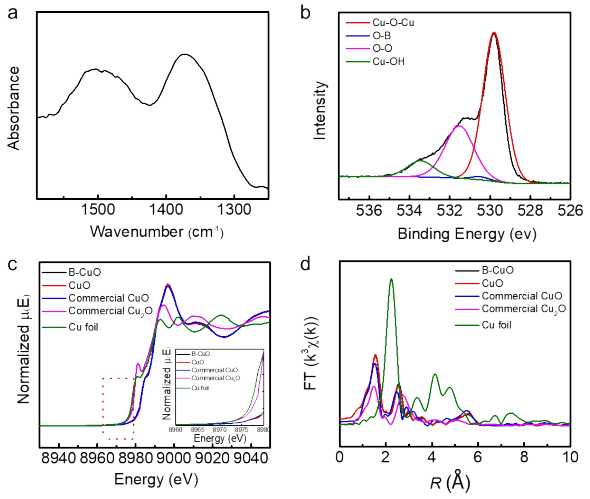

Fig. 2 FT-IR spectrum (a) and O1s XPS spectrum of B-CuO (b), Cu K-edge XANES spectra (c) and k^3-weighted χ (k) functions of the EXAFS spectra (d) of B-CuO, CuO, commercial CuO, Cu_2O and Cu foil.

The electrocatalytic performance of B-CuO for CO_2RR was detected. For comparison, the electrocatalytic performances of CuO and commercial CuO were also determined. Firstly, the CO_2 electrolysis of the three catalysts were determined by linear sweep voltammetry (LSV) acquired in CO_2-saturated 0.1 M $KHCO_3$ solution with a scan rate of 10 mV s^{-1}. As shown in Fig. 3a, B-CuO exhibits earlier onset potential in CO_2 saturated solutions than CuO and commercial CuO, implying its higher CO_2RR performance. The current density of B-CuO increases more sharply than the other two catalysts, indicating that it performs the best electrocatalytic activity for CO_2RR. B-CuO, CuO and commercial CuO show current densities of 18.2, 15.2 and 14.1 mA cm^{-2} (normalized by the geometrical surface area) at potential of -1.1 V (*vs*. RHE), respectively. The activities of the three catalysts for CO_2RR were evaluated in an H-type electrochemical cell separated by a Nafion 117 membrane. The gaseous and liquid products were analyzed by gas chromatography (GC) and ^{1}H nuclear magnetic resonance (^{1}H NMR) spectroscopy, respectively. There were only gaseous products (H_2, CO, ethylene) and no liquid product was detected in the potential range from -0.8 to -1.2 V (*vs*. RHE) (Fig. S5†). The FE of C_2H_4 reaches a maximum of 58.4% over B-CuO at -1.1 V (*vs*. RHE), which is much higher than the maximum FE of ethylene produced by CuO (17.2%) and commercial CuO (6.1%) (Fig. 3b). The CO produced by B-CuO is very small (FE_{CO} = 3.6%), while the FE_{CO} of CuO and commercial CuO are 24.8% and 17.3%, respectively (Fig. S6†). The selectivity to ethylene of the B-CuO synthesized in this work is higher than those of the reported B-doped Cu catalysts, which produced multiple C2 hydrocarbons such as ethanol.[24,26] The possible reason will be discussed in following.

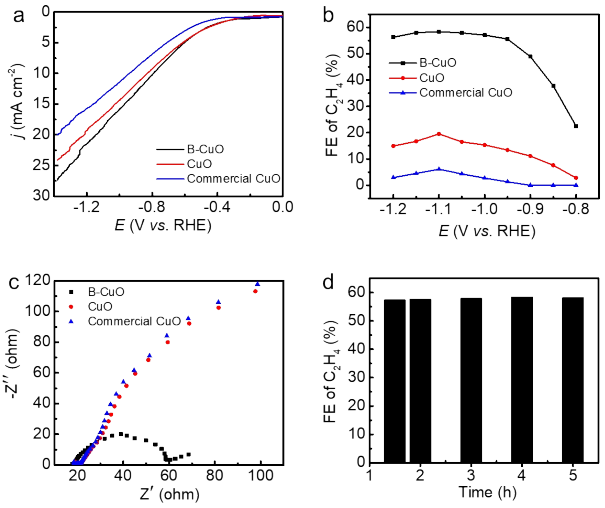

Fig. 3 LSV curves (a), FE of ethylene (b), and EIS spectra (c) of different catalysts, FE of ethylene of B-CuO with time at potential of -1.1 V *vs*. RHE (d).

Electrochemical impedance spectroscopy (EIS) measurement was performed to gain insight of reaction kinetics of CO_2RR on B-CuO, CuO and commercial CuO. A single fluid cell with 0.1 M $KHCO_3$ electrolyte was used and the frequencies are in the range of 10^{-1}-10^5 HZ. The Nyquist plots confirm that B-CuO possesses the smallest interfacial charge-transfer resistance and the fastest electron transfer among the three catalysts (Fig. 3c), suggesting the most favorable faradaic process.[41] The stability of the B-CuO for electrocatalysis was investigated. There is no decline for the FE of ethylene of B-CuO after 5 h of continuous electrolysis (Fig. 3d), indicating its stability can be well kept during catalysis.

On the basis of the above results, the possible reason for the high activity of the as-synthesized B-CuO is proposed. First, B-CuO has a nanowire structure, which favors the exposure of accessible active sites and facilitates the diffusion of CO_2 and electrocatalytic products[42]. Second, EXAFS results reveal the existence of abundant oxygen vacancies in B-CuO, which increase the binding affinities to the key intermediates that are favourable for electrocatalytic CO_2RR to ethylene[43]. Also, the existence of abundant oxygen vacancies would promote the adsorption of CO_2[43]. Our experiment shows that B-CuO has a much higher CO_2 adsorption capacity than CuO and commercial CuO (Fig. S7†). Owing to these unique features, the as-synthesized B-CuO shows a high activity for CO_2RR to ethylene.

The formation mechanism for the B-CuO electrocatalyst is very interesting. Its evolution process with reaction time was studied. At the early stage of 15 min, the sample presents as nanowires, with thickness of 10 nm and length of 1-3 μm (Fig. 4a). With the increasing reaction time, the nanowires begin to assemble to form nanobundles (Fig. 4b-d). XRD patterns (Fig. 4e) show that the sample formed at 15 min is copper hydroxide ($Cu(OH)_2$). At 30 min, the diffractions corresponding to CuO occur with the co-existence of a small amount of $Cu(OH)_2$, which completely converts to CuO at reaction time of 90 min. It is proposed that the copper ions in the solution interact with PEG to form a linear chain of ions, which can react with hydroxide rapidly to form $Cu(OH)_2$ nanowires. Subsequently, $Cu(OH)_2$ is dehydrated to form CuO nanowires, which assemble to nanobundles. During this process, boric acid is hydrolysed to form $[B(OH)_4]^-$, which could interact with copper ions and form Cu-O-B bond after dehydration and thus resulting in oxygen vacancies.[38-39,44,45] The performances of these samples synthesized at different reaction time for CO_2RR were also detected. It reveals that the B-CuO nanobundles with oxygen vacancies is the most selective for ethylene production (Fig. 4f).

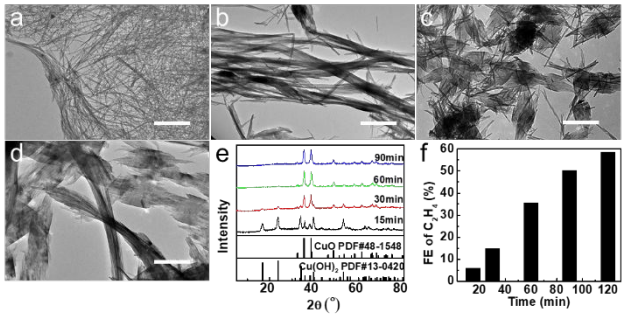

Fig. 4 TEM images of the products synthesized at reaction time of 15 min (a), 30 min (b), 60 min (c) and 90 min (d), corresponding XRD patterns (e) and maximum FE of C_2H_4. Scale bar: 400 nm.

The above results show that the B-doped CuO nanobundles have much improved activity and selectivity than the B-free CuO nanobundles. The effect of B content on catalytic effect was investigated. A series of CuO with different B contents were synthesized by varying the dosage of boric acid, while the other experimental conditions were the same with those for the above B-CuO. The B contents in those samples were determined by ICP-AES to be 0.04 wt%, 0.22 wt% and 0.54 wt%. The samples present similar morphologies (Fig. S8-S10†) with that of the above B-CuO with B content of 0.49 wt%. All these samples can catalyze CO_2RR to produce ethylene. The maximum FE of ethylene on the B-CuO with B content of 0.04 wt%, 0.22 wt%, 0.49 wt% and 0.54 wt% are 22.9%, 52.8%, 58.4% and 43.3%, respectively (Fig. S11†), which are 3.7, 8.7, 9.6 and 7.1 times higher than that of commercial CuO. Obviously, the FE of ethylene of B-CuO increases with increasing B content until 0.49 wt% and the increase of B content to 0.54 wt% cannot further improve the FE of ethylene. As evidenced by EXAFS results (Table S1), the B-CuO catalyst with B content of 0.49 wt% has the maximum oxygen vacancies. Thus, it exhibits the highest FE of ethylene for electrocatalytic CO_2RR.

Conclusions

In conclusion, we develop a novel electrocatalyst of B-doped CuO nanobundles for CO_2RR. The catalyst has a nanowire stack structure and abundant oxygen vacancies, which favor the exposure of accessible active sites, CO_2 adsorption and diffusion of CO_2 and electrocatalytic product. Owing to these unique features, the B-doped CuO nanobundles exhibit a highly selective performance for CO_2 conversion into ethylene.

Ethylene is the only multi-carbon product and its FE can reach 58.4% at -1.1 V (*vs*. RHE) with a current density of 18.2 mA cm^{-2}. This study provides a new strategy for producing single multi-carbon product from electrocatalytic CO_2RR by combining nano-engineering and hetero-atom doping.

Acknowledgements

The authors thank the financial supports from Ministry of Science and Technology of China (2017YFA0403003), National Natural Science Foundation of China (21525316, 21673254), Chinese Academy of Sciences (QYZDY-SSW-SLH013) and Beijing Municipal Science & Technology Commission (Z191100007219009).

Conflicts of interest

There are no conflicts to declare.

Notes and references

1 C. W. Lee, K. D. Yang, D. H. Nam, J. H. Jang, N. H. Cho, S. W. Im and K. T. Nam, *Adv. Mater.*, 2018, **30**, e1704717.
2 J. M. Spurgeon and B. Kumar, *Energy Environ. Sci.*, 2018, **11**, 1536.
3 A. Vasileff, C. Xu, Y. Jiao, Y. Zheng and S. Z. Qiao, *Chem*, 2018, **4**, 1809.
4 K. D. Yang, C. W. Lee, K. Jin, S. W. Im and K. T. Nam, *J. Phys. Chem. Lett.*, 2017, **8**, 538.
5 L. Zhang, Z. J. Zhao and J. Gong, *Angew. Chem., Int. Ed.*, 2017, **56**, 11326.
6 S. Ahn, K. Klyukin, R. J. Wakeham, J. A. Rudd, A. R. Lewis, S. Alexander, F. Carla, V. Alexandrov and E. Andreoli, *ACS. Catal.*, 2018, **8**, 4132.
7 F. N. Al-Rowaili, A. Jamal, M. S. Ba Shammakh and A. Rana, *ACS. Sustain. Chem. Eng.*, 2018, **6**, 15895.
8 Y. Y. Birdja, E. Pérez-Gallent, M. C. Figueiredo, A. J. Göttle, F. Calle-Vallejo and M. T. M. Koper, *Nat. Energy*, 2019, **4**, 732.
9 A. Bagger, W. Ju, A. S. Varela, P. Strasser and J. Rossmeisl, *ACS. Catal.*, 2019, **9**, 7894.
10 O. A. Baturina, Q. Lu, M. A. Padilla, L. Xin, W. Li, A. Serov, K. Artyushkova, P. Atanassov, F. Xu, A. Epshteyn, T. Brintlinger, M. Schuette and G. E. Collins, *ACS. Catal.*, 2014, **4**, 3682.
11 C. Choi, T. Cheng, M. Flores Espinosa, H. Fei, X. Duan, W. A. Goddard and Y. Huang, *Adv. Mater.*, 2019, **31**, e1805405.
12 C. M. Gabardo, C. P. O'Brien, J. P. Edwards, C. McCallum, Y. Xu, C. T. Dinh, J. Li, E. H. Sargent and D. Sinton, *Joule*, 2019, **3**, 2777.
13 D. Ren, Y. L. Deng, A. D. Handoko, C. S. Chen, S. Malkhandi and B. S. Yeo, *ACS. Catal.*, 2015, **5**, 2814.
14 C. H. Choi, K. Chung, T. T. H. Nguyen and D. H. Kim, *ACS. Energy. Lett.*, 2018, **3**, 1415.
15 W. Guo, X. Sun, C. Chen, D. Yang, L. Lu, Y. Yang and B. Han, *Green Chem.*, 2019, **21**, 503.
16 W. Ju, A. Bagger, G. P. Hao, A. S. Varela, I. Sinev, V. Bon, B. Roldan Cuenya, S. Kaskel, J. Rossmeisl and P. Strasser, *Nat. Commun.*, 2017, **8**, 944.
17 L. Lu, X. Sun, J. Ma, D. Yang, H. Wu, B. Zhang, J. Zhang and B. Han, *Angew. Chem., Int. Ed.*, 2018, **57**, 14149.
18 T. T. H. Hoang, S. Verma, S. Ma, T. T. Fister, J. Timoshenko, A. I. Frenkel, P. J. A. Kenis and A. A. Gewirth, *J. Am. Chem. Soc.*, 2018, **140**, 5791.
19 W. Zhu, L. Zhang, P. Yang, C. Hu, H. Dong, Z. J. Zhao, R. Mu and J. Gong, *ACS. Energy. Lett.*, 2018, **3**, 2144.
20 R. M. Aran-Ais, D. Gao and B. Roldan Cuenya, *Acc. Chem. Res.*, 2018, **51**, 2906.
21 S. Nitopi, E. Bertheussen, S. B. Scott, X. Liu, A. K. Engstfeld, S. Horch, B. Seger, I. E. L. Stephens, K. Chan, C. Hahn, J. K. Norskov, T. F. Jaramillo and I. Chorkendorff, *Chem. Rev.*, 2019, **119**, 7610.
22 Z. Q. Liang, T. T. Zhuang, A. Seifitokaldani, J. Li, C. W. Huang, C. S. Tan, Y. Li, P. De Luna, C. T. Dinh, Y. Hu, Q. Xiao, P. L. Hsieh, Y. Wang, F. Li, R. Quintero-Bermudez, Y. Zhou, P. Chen, Y. Pang, S. C. Lo, L. J. Chen, H. Tan, Z. Xu, S. Zhao, D. Sinton and E. H. Sargent, *Nat. Commun.*, 2018, **9**, 3828.
23 D. H. Nam, O. S. Bushuyev, J. Li, P. De Luna, A. Seifitokaldani, C. T. Dinh, F. P. Garcia de Arquer, Y. Wang, Z. Liang, A. H. Proppe, C. S. Tan, P. Todorovic, O. Shekhah, C. M. Gabardo, J. W. Jo, J. Choi, M. J. Choi, S. W. Baek, J. Kim, D. Sinton, S. O. Kelley, M. Eddaoudi and E. H. Sargent, *J. Am. Chem. Soc.*, 2018, **140**, 11378.
24 Y. Zhou, F. Che, M. Liu, C. Zou, Z. Liang, P. De Luna, H. Yuan, J. Li, Z. Wang, H. Xie, H. Li, P. Chen, E. Bladt, R. Quintero-Bermudez, T. K. Sham, S. Bals, J. Hofkens, D. Sinton, G. Chen and E. H. Sargent, *Nat. Chem.*, 2018, **10**, 974.
25 T. T. Zhuang, Z. Q. Liang, A. Seifitokaldani, Y. Li, P. De Luna, T. Burdyny, F. Che, F. Meng, Y. Min, R. Quintero-Bermudez, C. T. Dinh, Y. Pang, M. Zhong, B. Zhang, J. Li, P. N. Chen, X. L. Zheng, H. Liang, W. N. Ge, B. J. Ye, D. Sinton, S. H. Yu and E. H. Sargent, *Nat. Catal.*, 2018, **1**, 421.
26 C. J. Chen, X. F. Sun, L. Lu, D. X Yang, J. Ma, Q. G.Zhu, Q. L. Qian and B. X. Han, *Green Chem.*, 2018, **20**, 4579.
27 D. X. Tan, J. L. Zhang, L. Yao, X. N. Tan, X. Y. Cheng, Q. Wan, B. X. Han, L. R. Zheng and J. Zhang, *Nano Res.*, 2020, **13**, 768.
28 I. Ardelean and S. Cora, *J. Mater. Sci.: Mater. Electron.*, 2008, **19**, 584.
29 I. Ardelean, R. C. Lucacel and S. Cora, *Mod. Phys. Lett. B*, 2007, **21**, 2081.
30 E. Metwalli and *J. Non-Cryst. Solids*, 2003, **317**, 221.
31 L. V. Udod, K. A. Sablina, Y. N. Ivanov, G. A. Petrakovskii, A. Y. Koretz and A. F. Bovina, *Phys. Met. Metallogr*., 2005, **100**, S39.
32 B. V. R. Chowdari and Z. Rong, *Solid State Ionics*, 1996, **86-8**, 527.
33 T. Harada, H. Takebe and M. Kuwabara, *J. Am. Ceram. Soc.*, 2006, **89**, 247.
34 E. B. Simsek, *Appl. Catal. B*, 2017, **200**, 309.
35 P. Y. Shih, J. Y. Ding and S. Y. Lee, *Mater. Chem. Phys.*, 2003, **80**, 391.
36 P. Y. Shih, S. W. Yung and T. S. Chin, *J. Non-Cryst. Solids*, 1999, **244**, 211.
37 C. Zhu, A. Osherov and M. J. Panzer, *Electrochim. Acta*, 2013, **111**, 771.
38 J. Long, Q. Gu, Z. Zhang and X. Wang, *Prog. Chem.*, 2011, **23**, 2417.
39 M. Sakai, Y. Nagai, Y. Aoki and N. Takahashi, *Appl. Catal. A*, 2016, **510**, 57.
40 W. W. Wang, W. Z. Yu, P. P. Du, H. Xu, Z. Jin, R. Si, C. Ma, S. Shi, C. J. Jia and C. H. Yan, *ACS. Catal.*, 2017, **7**, 1313.
41 Y. Tan, P. Liu, L. Chen, W. Cong, Y. Ito, J. Han, X. Guo, Z. Tang, T. Fujita, A. Hirata and M. Chen, *Adv. Mater.*, 2014, **26**, 8023.
42 M. Ma, K, Djanashvili and W. A. Smith, *Angew. Chem., Int. Ed.*, 2016, **55**, 6680.
43 Z. X. Gu, N. Yang, P. Han, M. Kuang, B. B. Mei, Z. Jiang, J. Zhong, L. Li and G. F. Zheng, *Small Methods*, 2019, **3**, 1800449.
44 D. Grossmann, K. Klementiev, I. Sinev and W. Gruenert, *Chemcatchem*, 2017, **9**, 365.
45 W. W. Wang, P. P. Du, S. H. Zou, H. Y. He, R. X. Wang, Z. Jin, S. Shi, Y. Y. Huang, R. Si, Q. S. Song, C. J. Jia and C. H. Yan, *ACS. Catal.*, 2015, **5**, 2088.